Since January 2020 Elsevier has created a COVID-19 resource centre with free information in English and Mandarin on the novel coronavirus COVID-19. The COVID-19 resource centre is hosted on Elsevier Connect, the company's public news and information website.

Journal of Molecular Liquids 335 (2021) 116250

Contents lists available at ScienceDirect

Journal of Molecular Liquids

journal homepage: www.elsevier.com/locate/molliq

Charge-transfer chemistry of azithromycin, the antibiotic used worldwide to treat the coronavirus disease (COVID-19). Part III: A green protocol for facile synthesis of complexes with TCNQ, DDQ, and TFQ acceptors

Abdel Majid A. Adam [a,*], Hosam A. Saad [a], Amnah M. Alsuhaibani [b], Moamen S. Refat [a], Mohamed S. Hegab [c]

[a] Department of Chemistry, College of Science, Taif University, P.O. Box 11099, Taif 21944, Saudi Arabia
[b] Department of Physical Sport Science, Princess Nourah bint Abdulrahman University, Riyadh, Saudi Arabia
[c] Deanship of Supportive Studies (D.S.S.), Taif University, P.O. Box 11099, Taif 21944, Saudi Arabia

ARTICLE INFO

Article history:
Received 26 January 2021
Revised 14 February 2021
Accepted 22 February 2021
Available online 22 April 2021

Keywords:
Charge-transfer
Azithromycin
TCNQ
DDQ
TFQ
Eco-friendly
SARS-CoV-2
COVID-19

ABSTRACT

Investigating the chemical properties of molecules used to combat the COVID-19 pandemic is of vital and pressing importance. In continuation of works aimed to explore the charge-transfer chemistry of azithromycin, the antibiotic used worldwide to treat COVID-19, the disease resulting from infection with the novel SARS-CoV-2 virus, in this work, a highly efficient, simple, clean, and eco-friendly protocol was used for the facile synthesis of charge-transfer complexes (CTCs) containing azithromycin and three π-acceptors: 7,7,8,8-tetracyanoquinodimethane (TCNQ), 2,3-dichloro-5,6-dicyano-*p*-benzoquinone (DDQ), and tetrafluoro-1,4-benzoquinone (TFQ). This protocol involves grinding bulk azithromycin as the donor (D) with the investigated acceptors at a 1:1 M ratio at room temperature without any solvent. We found that this protocol is environmentally benign, avoids hazardous organic solvents, and generates the desired CTCs with excellent yield (92–95%) in a straightforward means.

1. Introduction

Coronaviruses (CoVs) belong to the Coronaviridae family and Coronavirinae subfamily, which is composed of four genera, δ-CoVs, γ-CoVs, β-CoVs, and α-CoVs. The first CoV outbreak in humans occurred in China in 2003 and was termed severe acute respiratory syndrome coronavirus (SARS-CoV). The second outbreak, known as Middle East respiratory syndrome coronavirus (MERS-CoV), was first identified in the Middle East in 2012 [1,2]. The third outbreak, first described in Wuhan, China on December 9, 2019, was caused by a novel CoV named SARS coronavirus 2 (SARS-CoV-2). This most recent outbreak is the first with pandemic potential in non-immune populations in the 21st century [3]. SARS-CoV-2, believed to have originated from a seafood market in Wuhan, spread very quickly throughout China and then around the globe, thereby causing a destabilizing global pandemic [4]. The World Health Organization (WHO) named the disease caused by this novel virus the Coronavirus disease 2019 (COVID-19) and announced it as a global pandemic on March 12, 2020 [5]. One year later, more than 93 million people worldwide have been definitively diagnosed with COVID-19 (23.6 million in the USA), 2 million of which have since died. To date, no gold standard treatment or vaccine exists to effectively combat this contagious, life-threatening condition. Many pharmacologically effective molecules are being investigated for antiviral efficacy against SARS-CoV-2 (e.g., lopinavir/ritonavir, remdesivir, tocilizumab, azithromycin, hydroxychloroquine, chloroquine, etc.). Azithromycin, a member of the macrolide class of antibiotics, has shown promising results when used to treat COVID-19 (Fig. 1a). Azithromycin has a broad spectrum of antibacterial properties that render it highly effective against both G + and G- bacteria. Moreover, its anti-inflammatory, antiviral, immunomodulatory, and antimalarial properties make it particularly well-suited to not only reign in this novel, highly contagious virus but also to mitigate the life-threatening symptoms (i.e., COVID-19) associated with its infection [6-9]. The use of this antibiotic has been strongly recommended and widely implemented to treat COVID-19 worldwide,

* Corresponding author.
E-mail address: majidadam@tu.edu.sa (A.M.A. Adam).

https://doi.org/10.1016/j.molliq.2021.116250
0167-7322/

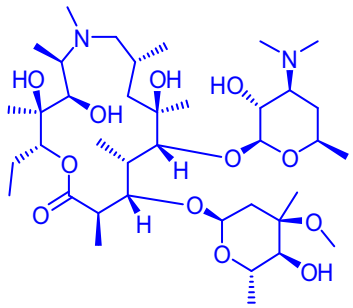

Fig. 1a. Structure of the azithromycin molecule.

either alone or in combination with chloroquine and its derivative hydroxychloroquine [10-18].

Charge-transfer complexes (CTCs) contribute to many important applications in biology, chemistry, physics, and industry [19-40]. Every year, extensive research efforts are dedicated to producing new CTCs, investigating their properties (e.g., kinetic, photophysical, thermodynamic, crystallographic, spectral), determining which factors affect the CT interactions (e.g., time, temperature, type of solvent, time, concentration), and exploring and developing novel applications [26,41-64]. Exploring the modifiability of azithromycin and the chemistry underlying the formation of these novel derivatives could provide insight into the mechanisms underlying this antibiotic's efficacy, which could help to optimize its application to the treatment of COVID-19. As a continuation of our previous works [65,66] that aim to furnish a big-picture perspective on the CT chemistry of azithromycin by examining its interactions with several σ- and π-acceptors and the resultant CTCs, in this work, we describe a highly efficient, straightforward, and environmentally friendly protocol for the facile synthesis of CTCs between azithromycin and three π-acceptors (TCNQ, DDQ, and TFQ; Fig. 1b).

2. Experimental

2.1. Reagents

The starting reagents used for the synthesis of the CTCs were commercially available and analytical grade chemicals obtained from BDH (United Kingdom) and Sigma-Aldrich (USA) chemical companies and used without any additional purification. Azithromycin powder ($C_{38}H_{72}N_2O_{12}$; 748.98 g/mol; purity ≥ 98%) was used as the donor and complexed with three π-acceptors: 7,7,8,8-tetra cyanoquinodimethane (TCNQ; $C_{12}H_4N_4$; 204.19 g/mol; purity 98%), 2,3-dichloro-5,6-dicyano-*p*-benzoquinone (DDQ; $C_8Cl_2N_2O_2$; 227.00 g/mol; purity 98%), and tetrafluoro-1,4-benzoquinone (TFQ; $C_6F_4O_2$; 180.06 g/mol; purity 97%).

2.2. Analytical instrumentation

The elemental composition of the synthesized CTCs were analyzed using a Perkin-Elmer 2400CHN Elemental Analyzer to determine their hydrogen, carbon, and nitrogen content (%). The NMR (^{1}H and ^{13}C), FTIR, and UV–visible spectra of the synthesized CTCs were registered with Bruker DRX-250 Digital FT-NMR, Shimadzu FTIR, and Perkin – Elmer Lambda 25 UV/Vis spectrophotometers, respectively, at room temperature. The electronic spectra were collected from the CTCs solubilized in methanol from 200 to 800 nm, while solid-state CTCs were used to collect FTIR spectra in the 400 to 4000 cm^{-1} range. At 400 MHz, the Bruker DRX-250 instrument generated the ^{1}H and ^{13}C NMR spectra of the solid-state CTCs in DMSO d_6 solution, where the chemical shift values are presented in δ scale relative to the internal reference tetramethylsilane (TMS).

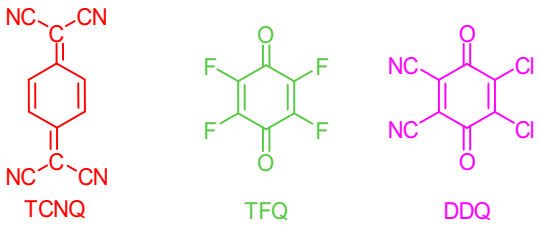

Fig. 1b. Structures of the investigated π-acceptors.

2.3. Synthetic protocol

Complexation of the azithromycin donor with the TCNQ, DDQ, and TFQ acceptors was attempted by grinding their solid powders on a dry, clean porcelain mortar using a pestle under the following reaction conditions:

- Starting reagent: solvent-free, solid–solid interaction
- Temperature: ambient
- Time: ~3 min
- Stoichiometry: 1:1 (donor to acceptor)

3. Results and discussion

3.1. Preliminary steps

Three preliminary steps should be conducted prior to preparing the CTCs of azithromycin by the solid–solid interaction. These steps are: i) observe whether a color change occurs upon mixing azithromycin with each acceptor in solution, ii) analyze the λ_{CT} of the CTCs in solution by UV–visible spectroscopy, and iii) verify the composition of azithromycin and each acceptor in solution for use in the preparation of the CTCs through solid–solid interactions.

3.1.1. Color change

Before preparing the azithromycin-based CTCs using solid–solid interactions, it's necessary to observe the CT interaction between the solubilized azithromycin donor molecule and TCNQ, DDQ, and TFQ acceptors. The physical property most indicative of a CT interaction is color, which changes upon combining the donor and acceptor. To observe the changing color after mixing azithromycin with each of the acceptors, solutions of azithromycin and the acceptors were prepared at a concentration of 1×10^{-3} M in methanol solvent. The free azithromycin solubilized in methanol was coreless. In methanol solvent, the TCNQ acceptor had a light green color, the DDQ acceptor had a brown color, and the TFQ acceptor had a pale brown color. Striking color changes visible to the naked eye occurred when azithromycin was mixed with each acceptor at ambient temperature at a 1:1 ratio. The color changed from light green to pale brown in the resultant CTC with TCNQ (Fig. 2), from brown to intense red in the resultant CTC with DDQ (Fig. 3), and from pale brown to canary yellow in the resultant CTC with TFQ (Fig. 4). These types of color changes are indicative of strong CT interactions between azithromycin and all of the acceptors, reflecting the strong donating property of azithromycin and the strong accepting properties of TCNQ, DDQ, and TFQ. Indeed, the azithromycin molecule bears several electron-donating groups such as methoxy, hydroxy, ether, and carbonyl groups, as well as two nitrogen atoms [$-NCH_3$, $-N(CH_3)_2$]. The TCNQ, DDQ, and TFQ acceptor molecules contain different types of electron-withdrawing groups. The TCNQ molecule has one type of electron-withdrawing group (four cyano groups). The TFQ mole-

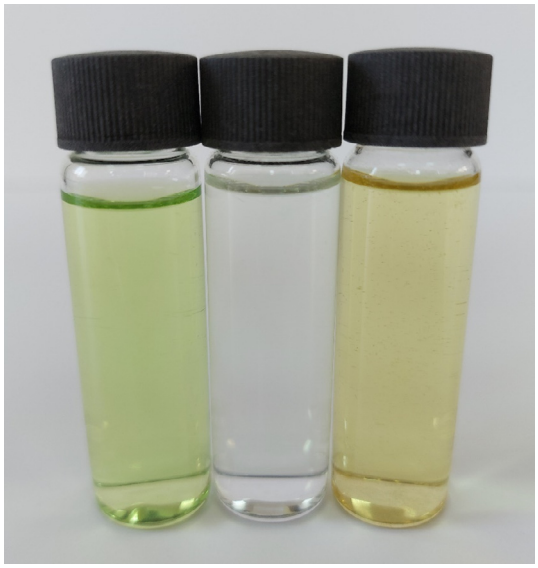

Fig. 2. Pronounced color change upon mixing TCNQ acceptor (*far left*; *light green*) with azithromycin (*middle; colorless*) to produce the CT complex (*far right*; *pale brown*) in the methanol solvent.

Fig. 3. Pronounced color change upon mixing DDQ acceptor (*far left*; *brown*) with azithromycin (*middle; colorless*) to produce the CT complex (*far right*; *intense red*) in the methanol solvent.

cule has two types of electron-withdrawing groups (two carbonyl groups and four fluorine groups), while the DDQ molecule has three types of electron-withdrawing groups (two cyano groups, two carbonyl groups, and two chloro groups). The presence of three different types of electron-withdrawing groups in the DDQ molecule greatly decreases the electron density of its aromatic ring, thereby rendering the DDQ molecule a robust, very strong electron-accepting system that resulted in the formation of the distinctive intense red color with azithromycin, compared with the pale brown color formed with the TCNQ acceptor and canary yellow color formed with the TFQ acceptor. The intensity of the color of the resultant CTC increased with the types of electron-accepting groups in the acceptor molecule. This increase was as follows: pale brown (TCNQ; one type) < canary yellow (TFQ; two types) < intense red (DDQ; three types).

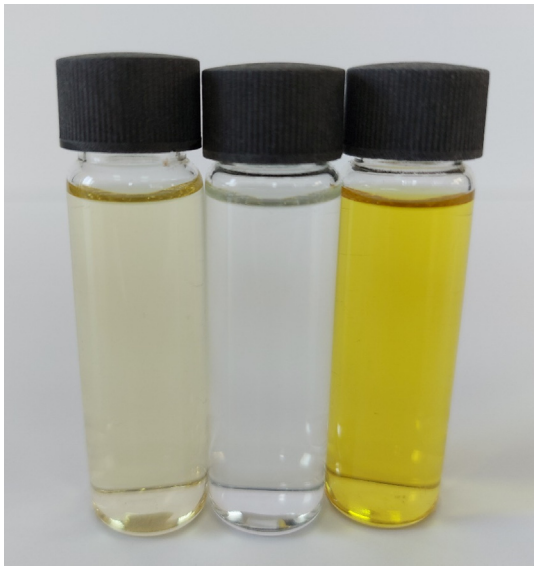

Fig. 4. Pronounced color change upon mixing TFQ acceptor (*far left*; *pale brown*) with azithromycin (*middle; colorless*) to produce the CT complex (*far right*; *canary yellow*) in the methanol solvent.

3.1.2. Observing the CT bands

After observing the color change that resulted from the interaction of azithromycin with TCNQ, DDQ, and TFQ, it was necessary to observe the CT bands (shape, position, λ_{CT}) that characterized the resultant CTCs in solution using UV–visible spectroscopy. To observe the characteristics of the CT bands, solutions of azithromycin and the acceptors were prepared at concentrations of 5×10^{-4} M in methanol and these were scanned with a UV–visible spectrophotometer from 200 to 800 nm at ambient temperature. The electronic absorption of free azithromycin, free acceptor (TCNQ, DDQ, or TFQ), and the CTC derived by mixing the two solutions (1:1) are presented in Figs. 5a-c. Free azithromycin in methanol had no measurable absorption bands in the UV–visible region. The free TCNQ acceptor solubilized in methanol had a very strong, broad absorption band that ranged from 300 to 450 nm with a λ_{max} of 393 nm. Upon complexation between TCNQ and the donor, this band disappeared and a new, very strong, broad band appeared from 285 to 375 nm, centered at λ_{CT} 336 nm. The free DDQ acceptor had a strong, sharp absorption band at 295 nm with a long tail

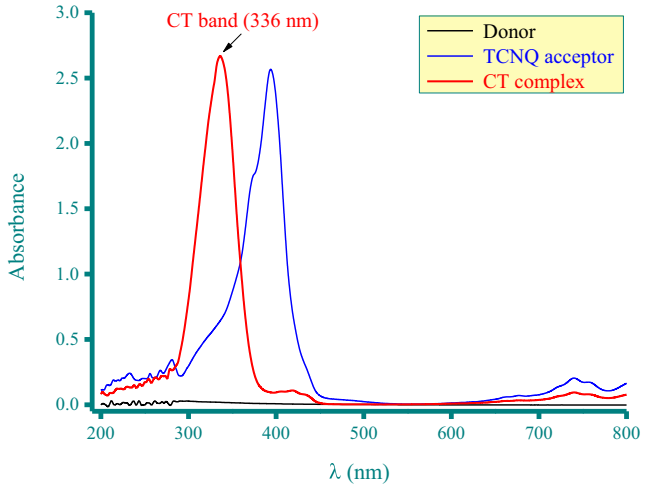

Fig. 5a. The UV–visible spectra of the donor (azithromycin), the TCNQ acceptor, and resultant CT complex in methanol solvent.

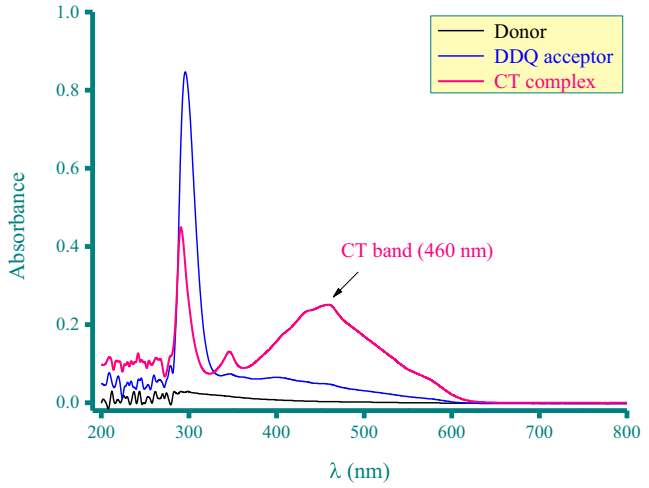

Fig. 5b. The UV–visible spectra of the donor (azithromycin), the DDQ acceptor, and resultant CT complex in methanol solvent.

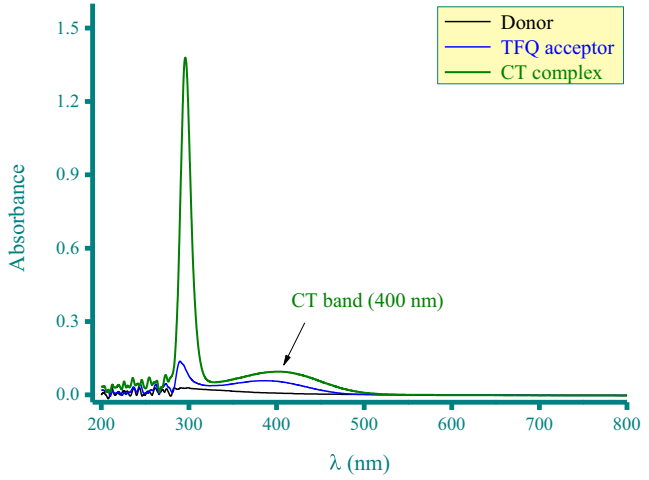

Fig. 5c. The UV–visible spectra of the donor (azithromycin), the TFQ acceptor, and resultant CT complex in methanol solvent.

ranging from 340 to 600 nm, gradually decreasing in intensity. After DDQ interacted with the donor, the intensity of this band decreased greatly with a slight shift in its maximum to 290 nm. The decreased intensity of the characteristic band of DDQ was coupled with the formation of a new, strong, broad absorption band that ranged from 360 to 600 nm, centered at λ_{CT} 460 nm. The free TFQ acceptor had two weak absorption bands: a narrow band at 290 nm and a wide band that ranged from 330 to 460 nm, centered at λ_{CT} 385 nm. Upon complexing TFQ with the donor, the intensity of the narrow band located at 290 nm greatly increased, about 10-fold, and slightly shifted its maximum to 296 nm. The intensity of the wide band centered at 385 nm also increased, becoming broader with a maximum shifted to λ_{CT} 400 nm. These spectral results indicate that the complexation of the donor with the TCNQ and DDQ acceptors was characterized by the formation of a new band where neither the free donor nor acceptor previously had any measurable absorption (hypsochromic shifts), while the complexation with the TFQ acceptor was characterized by the increased intensity and size of the absorption band that characterized the free TFQ (bathochromic shift).

3.1.3. Composition of the interaction

The third preliminary step is to verify the composition of the interaction between the donor and TCNQ, DDQ, and TFQ acceptors in solution using the spectrophotometric titration method [67] and Job's continuous variation method [68]. The molar ratio (donor to acceptor) derived using these two methods will be used to prepare the CTCs with azithromycin by solid–solid interaction. Fig. 6a presents the curves obtained from the spectrophotometric titration method. These curves were derived by plotting the absorbances (λ_{CT}) of a series of 10 solutions containing molar ratios ranging from 4:1 to 1:4 donor to acceptor against the corresponding acceptor volume. The curves in Fig. 6a show the intersection of the resultant two straight lines corresponded to an acceptor volume of 1.0 mL, indicating that the interaction between the donor and all of the acceptors occurred at a 1:1 M ratio. Fig. 6b presents the curves obtained using Job's continuous variation method. These curves were derived by plotting the absorbances (λ_{CT}) of a series of 10 solutions containing varied molar fractions ($C_D + C_A$) of the donor and acceptor against the corresponding molar fraction of the acceptor [$\chi_A = C_A/(C_D + C_A)$]. The curves in Fig. 6b show that the maximum absorbance corresponded to a molar fraction of 0.50, reflecting that the donor formed a 1:1 CTC with each of the

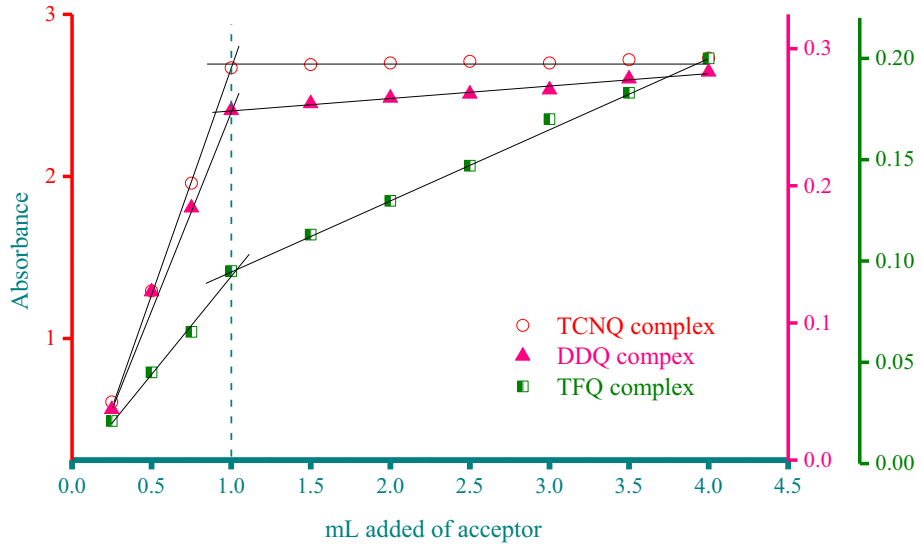

Fig. 6a. Composition of the interaction between azithromycin with acceptors determined by spectrophoometric titration method.

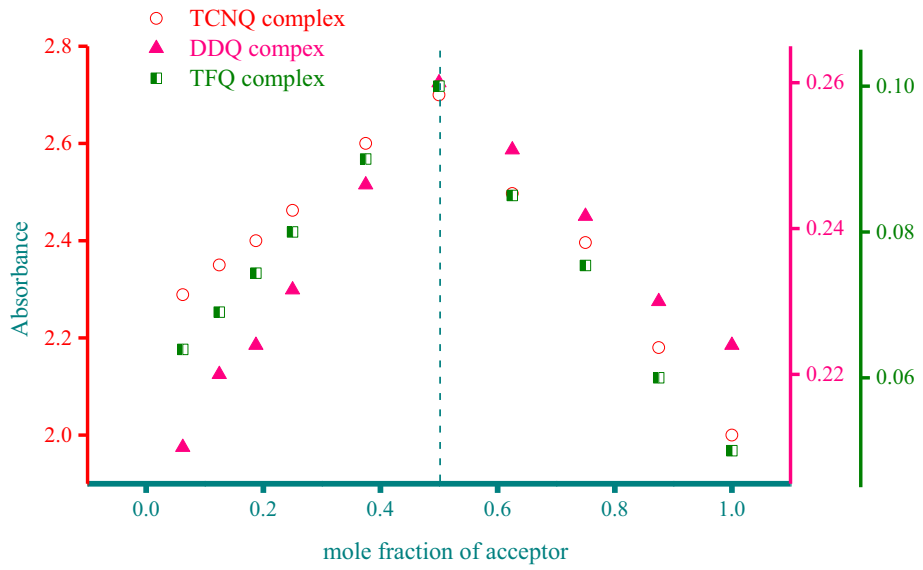

Fig. 6b. Composition of the interaction between azithromycin with acceptors determined by Job's continuous variation method.

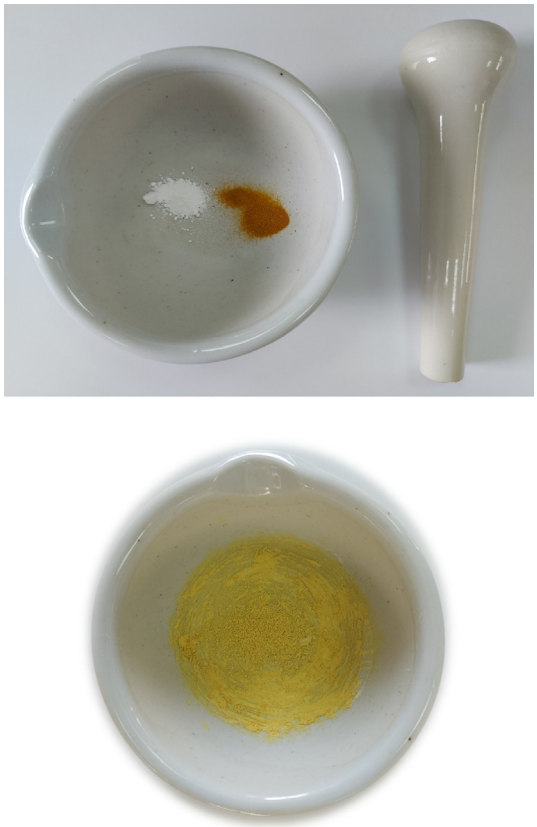

Fig. 7a. TCNQ complex generated by grinding azithromycin (white powder) and TCNQ (brown powder) for 3 min.

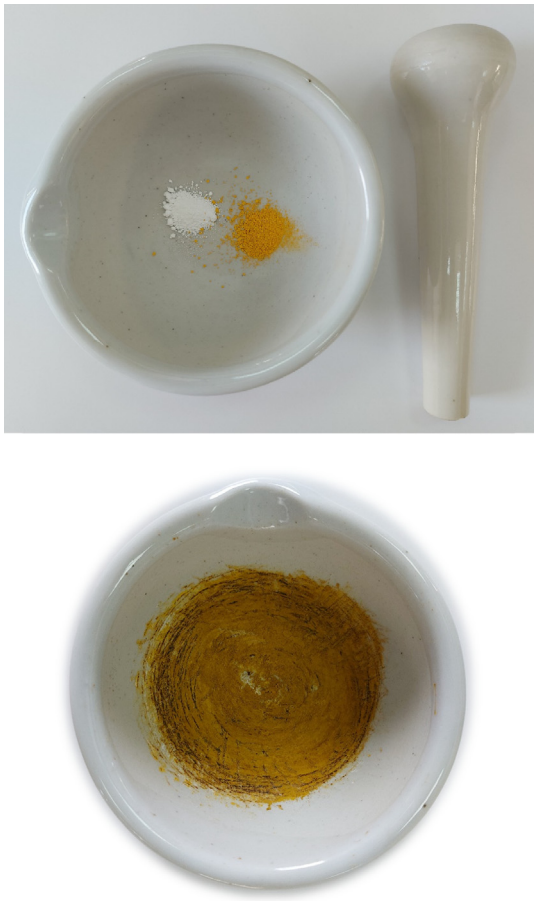

Fig. 7b. DDQ complex generated by grinding azithromycin (white powder) and DDQ (light brown powder) for 3 min.

acceptors. In conclusion, the results from both methods agreed and confirmed that azithromycin reacted with the TCNQ, DDQ, and TFQ acceptors via a 1:1 M ratio.

3.2. Methodology

CTCs of azithromycin with TCNQ, DDQ, and TFQ acceptors were produced using a fast, clean, and straight-forward two-step method based on mortar-grinding their solids under four conditions: i) solvent-free solid–solid reaction type, ii) ambient reaction temperature, iii) ~ 3 min reaction time, and iv) 1:1 (donor to acceptor) reaction stoichiometry. A pronounced color change was observed after grinding the pair of compounds (donor and

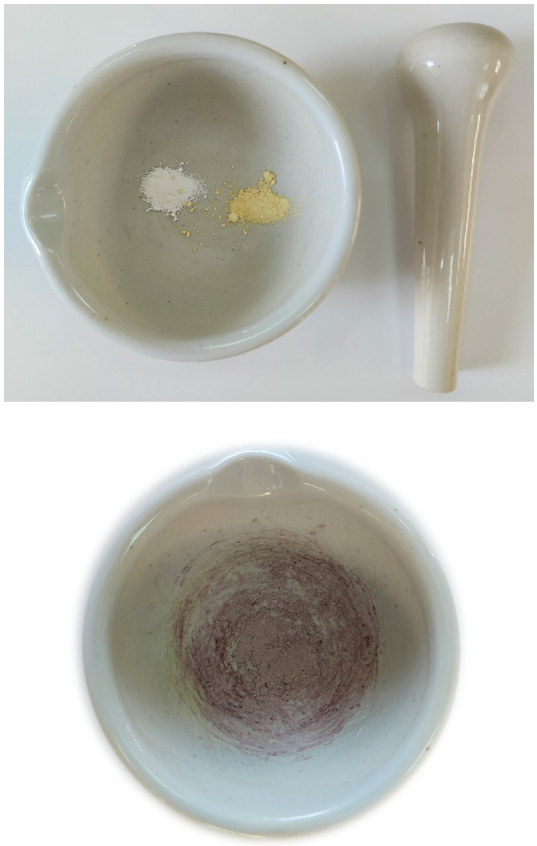

Fig. 7c. TFQ complex generated by grinding azithromycin (white powder) and TFQ (light yellow powder) for 3 min.

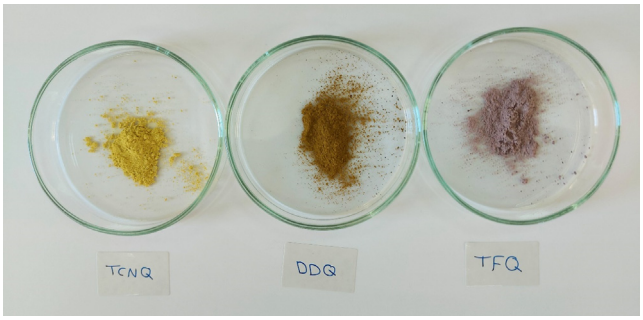

Fig. 8. TCNQ, DDQ, and TFQ complexes after rinsing with 5 mL diethyl ether and drying.

acceptor) for ~ 1 min, as shown in Figs. 7a-c. The grinding was continued for 2 min to ensure the completeness of the reaction and the homogeneity of the solid product. Next, the crude solid homogenates were rinsed with 5 mL of diethyl ether to remove any unreacted compounds and then dried with a water pump. The complex obtained with TCNQ had a light-brown color, with DDQ had a dark-brown color, while the TFQ CTC had a light-violet color, as depicted in Fig. 8.

3.3. Characterization data of the CTCs

The generated CTCs were characterized by UV–visible, FTIR, ^{1}H NMR, ^{13}C NMR spectral data as well as elementary data. Figs. 9a-c contains UV–visible spectra of the synthesized CTCs. The FTIR of the free donor and acceptor molecules are presented in Figs. 10a-

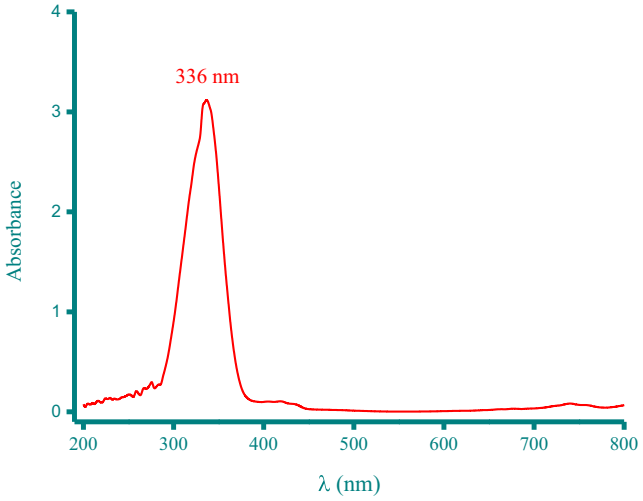

Fig. 9a. The UV–visible spectrum of TCNQ complex (5.0×10^{-4} M) in methanol solvent.

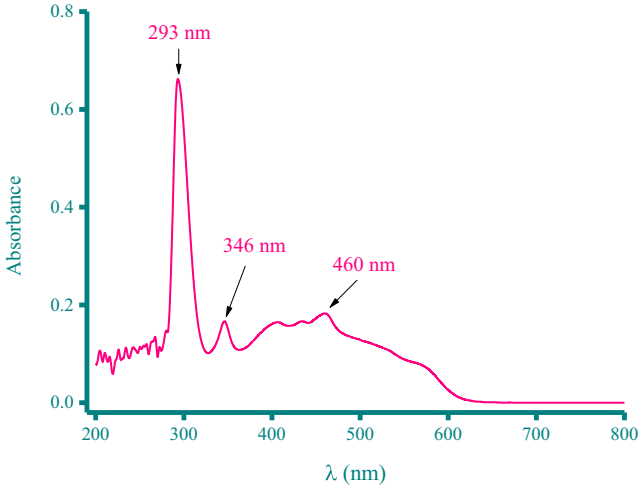

Fig. 9b. The UV–visible spectrum of DDQ complex (5.0×10^{-4} M) in methanol solvent.

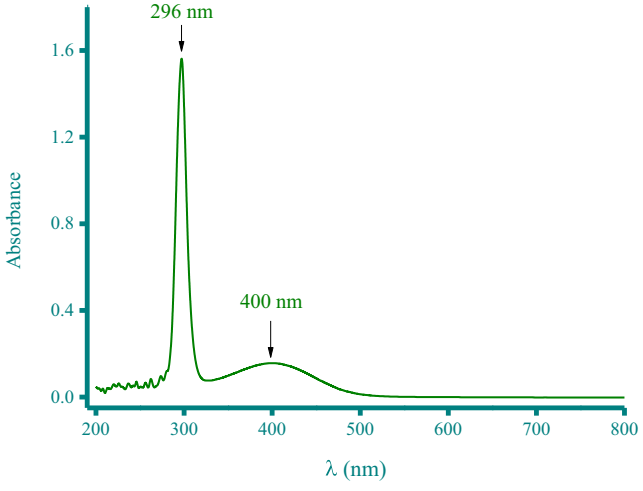

Fig. 9c. The UV–visible spectrum of TFQ complex (5.0×10^{-4} M) in methanol solvent.

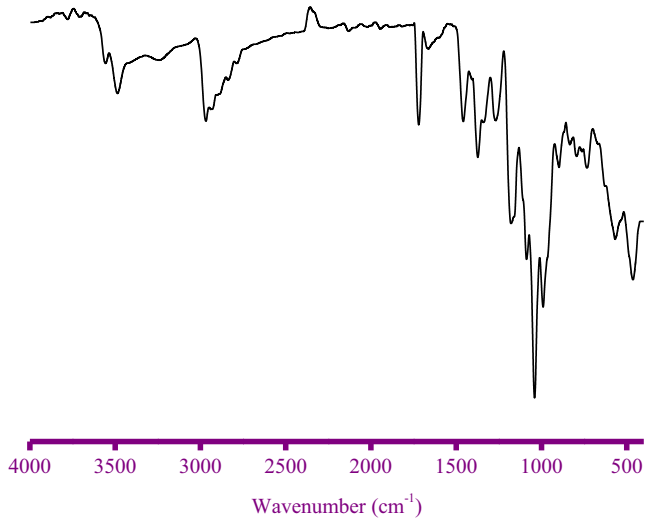

Fig. 10a. FTIR spectrum of the free azithromycin molecule.

Fig. 10b. FTIR spectrum of the free TCNQ molecule.

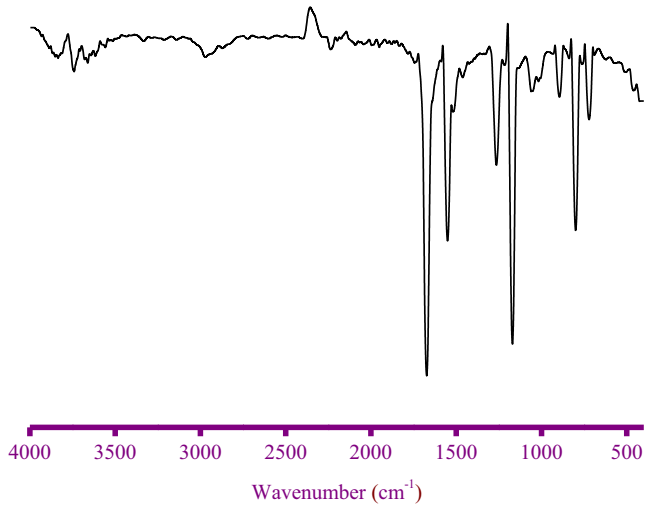

Fig. 10c. FTIR spectrum of the free DDQ molecule.

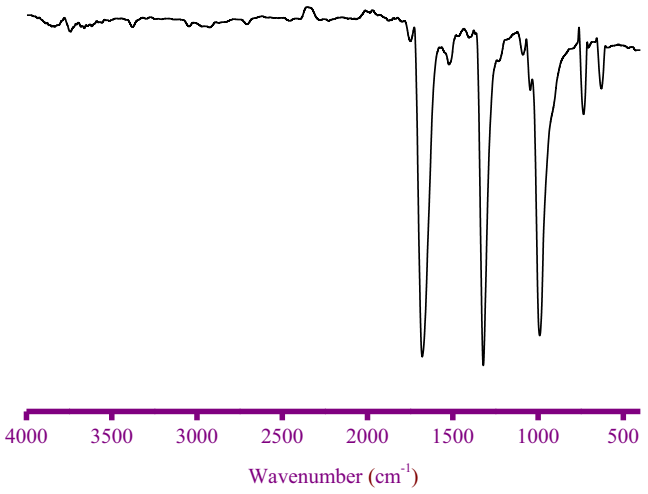

Fig. 10d. FTIR spectrum of the free TFQ molecule.

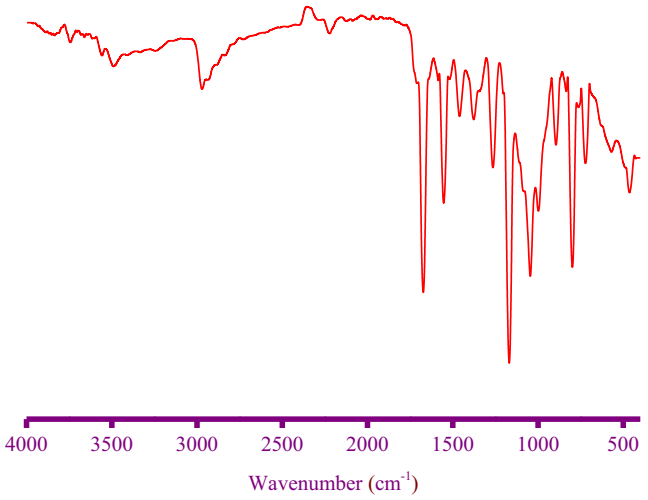

Fig. 11a. FTIR spectrum of the TCNQ complex.

Fig. 11b. FTIR spectrum of the DDQ complex.

d. Figs. 11a-c contains the FTIR spectra of the synthesized CTCs. Fig. S1 presents the structure of free azithromycin along with its atom numbers to facilitate interpreting the ^{1}H and ^{13}C NMR

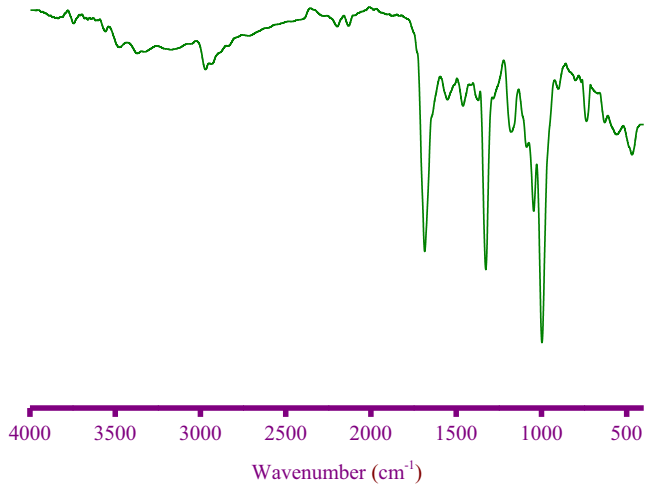

Fig. 11c. FTIR spectrum of the TFQ complex.

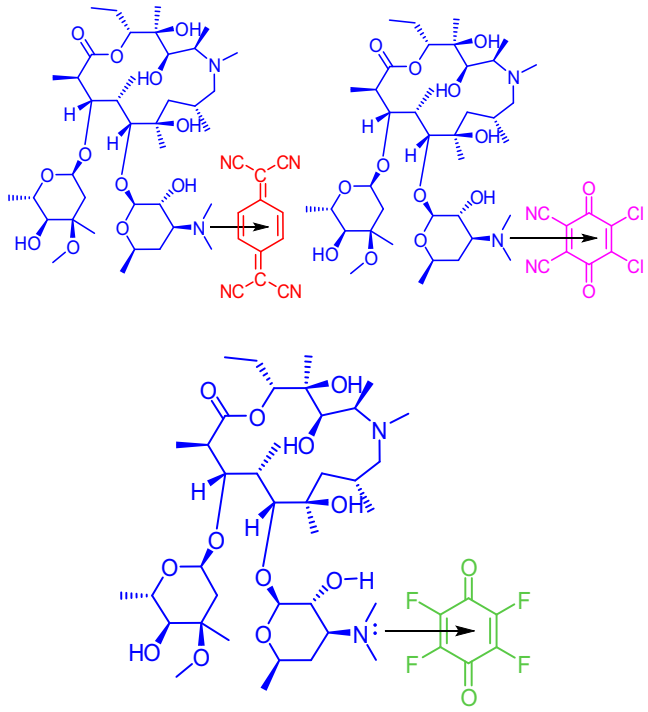

Fig. 12. Proposed structures of the synthesized CTCs.

spectra for the synthesized CTCs given in Fig. S2-S5. The elemental and spectral data collected for the CTCs were:

3.3.1. Free azithromycin

White powder; CHN elemental data: $C_{38}H_{72}N_2O_{12}$ (748.98 g mol^{-1}); Calculated (%): C 60.88; H 9.61; N 3.74. FTIR data (cm^{-1}): 570, 737, 797, 836, 895, 992, 1040, 1083, 1181, 1269, 1377, 1465, 1660, 1719, 2834, 2883, 2932, 2971, 3245, 3490. ^{1}H NMR data (400 MHz, DMSO d_6) (ppm): δ = 5.61 (t, 1H, (C_2-C<u>H</u>)), 5.55 (t, 1H, (C_2–C<u>H</u>)), 5.22 (d, 1H, J = 4.4, ($C_{2''}$–C<u>H</u>)), 5.02 (m, 1H, ($C_{6'}$–C<u>H</u>)), 4.96 (dd, 1H, (C_{13}-C<u>H</u>)), 4.85 (d, 1H, J = 5.2, (C_{11}-C<u>H</u>)), 4.77 (d, 1H, J = 3.2, (C_4-C<u>H</u>)), 4.67 (m, 1H, ($C_{6''}$–C<u>H</u>)), 4.60 (s, 3H, ($C_{4''}$–C<u>H</u>$_3$)), 4.55 (dd, 1H, ($C_{3''}$–C<u>H</u>)), 4.33 (s, 5H, 5OH), 4.02 (d, 1H, J = 6.8, ($C_{5'}$–C<u>H</u>)), 3.96 (d, 2H, J = 5.2, (C_7-C<u>H</u>$_2$)), 3.81 (m, 1H, (C_{14}-C<u>H</u>)), 3.77 (m, 1H, (C_5-C<u>H</u>)), 3.47 (m, 1H, ($C_{4''}$–C<u>H</u>)), 3.20 (s, 3H, (N_6-C<u>H</u>$_3$), 2.99 (s, 6H, ($C_{4''}$-N(C<u>H</u>$_3$)$_2$), 2.67 (m, 1H, (C_{12}-C<u>H</u>)), 2.45 (d, 2H, J = 4.6, (C_9-C<u>H</u>$_2$)), 2.26 (dd, 2H, ($C_{5''}$–C<u>H</u>$_2$)), 2.01 (m, 1H, (C_8-C<u>H</u>)), 1.71 (d, 2H, J = 3.2, ($C_{3'}$–C<u>H</u>$_2$)), 1.60 (m, 2H, (C_2-C<u>H</u>$_2$CH$_3$)), 1.56 (d, 3H, J = 6.2, ($C_{6'}$–C<u>H</u>$_3$)), 1.30 (s, 3H, (C_{10}-C<u>H</u>$_3$)), 1.27 (s, 3H, ($C_{4'}$–C<u>H</u>$_3$)), 1.01 (d, 3H, J = 5.6, ($C_{6''}$–C<u>H</u>$_3$)), 0.94 (d, 3H, J = 4.8, (C_{14}-C<u>H</u>$_3$)), 0.89 (d, 3H, J = 5.2, (C_{12}-C<u>H</u>$_3$)), 0.82 (s, 3H, (C_3-C<u>H</u>$_3$)), 0.79 (d, 3H, J = 4.4, (C_5-C<u>H</u>$_3$)), 0.67 (d, 3H, J = 3.2, (C_8-C<u>H</u>$_3$)), 0.58 (t, 3H, (C_2-CH$_2$C<u>H</u>$_3$)). ^{13}C NMR data (100 MHz, DMSO d_6) (ppm): δ = 177.66 (C_{15}-<u>C</u> = O), 102.00 ($C_{2''}$–<u>C</u>H), 94.89 ($C_{2'}$–<u>C</u>H), 85.50 (C_{11}-<u>C</u>), 80.23 (C_4-<u>C</u>H), 79.71 (C_{13}-<u>C</u>), 77.82 ($C_{5'}$–<u>C</u>H), 77.76 (C_2-<u>C</u>H), 74.01 (C_{10}-<u>C</u>), 73.29 (C_4-<u>C</u>), 72.11 (C_3-<u>C</u>), 70.91 ($C_{3''}$–<u>C</u>H), 69.74 ($C_{6''}$–<u>C</u>H), 65.40 ($C_{4''}$–<u>C</u>H), 65.29 (C_6–<u>C</u>H), 62.56 (C_5-<u>C</u>H), 56.40 (C_7-<u>C</u>H$_2$), 49.29 ($C_{4''}$–O<u>C</u>H$_3$), 45.17 (C_{14}-<u>C</u>H), 42.01(N_6-<u>C</u>H$_3$), 40.62 ($C_{3''}$-*N*(2<u>C</u>H$_3$)), 38.48 (C_{12}-<u>C</u>H), 36.48 (C_9-<u>C</u>H), 34.98 ($C_{3'}$–<u>C</u>H$_2$), 30.37 (C_8-<u>C</u>H), 28.60 ($C_{5''}$–<u>C</u>H$_2$), 25.55 (C_{10}-<u>C</u>H$_3$), 22.41 ($C_{4'}$–<u>C</u>H$_3$), 21.63 (C_2-<u>C</u>H$_2$CH$_3$), 21.49 ($C_{6''}$–<u>C</u>H$_3$), 21.28 (C_8-<u>C</u>H$_3$), 18.81 (C_3-<u>C</u>H$_3$), 18.04 (C_6–<u>C</u>H$_3$), 15.23 (C_{15}-<u>C</u>H$_3$), 11.70 (C_5-<u>C</u>H$_3$), 11.42 (C_2-CH$_2$<u>C</u>H$_3$), 9.36 (C_{12}-<u>C</u>H$_3$).

3.3.2. TCNQ complex

Light brown-colored powder; yield 95%; CHN elemental data: $C_{50}H_{76}N_6O_{12}$ (953.17 g mol^{-1}); Observed (%): C 63.14; H 7.80; N 9.05. Calculated (%): C 62.95; H 7.97; N 8.81. UV–visible data (nm): 336. FTIR data (cm^{-1}): 461, 570, 726, 796, 893, 998, 1040, 1172, 1267, 1380, 1460, 1555, 1677, 2224, 2284, 2826, 2885, 2933, 2972, 3236, 3487. ^{1}H NMR data (400 MHz, DMSO d_6) (ppm): δ = 7.55 (s, 4H, TCNQ ring *H*), 5.74 (t, 1H, (C_2-C<u>H</u>)), 5.69 (t, 1H, (C_2–C<u>H</u>)), 5.37 (d, 1H, ($C_{2''}$–C<u>H</u>)), 5.11 (m, 1H, ($C_{6''}$–C<u>H</u>)), 4.95 (dd, 1H, (C_{13}-C<u>H</u>)), 4.81 (d, 1H, J = 5.6, (C_{11}-C<u>H</u>)), 4.83 (d, 1H, J = 5.4, (C_4-C<u>H</u>)), 4.72 (m, 1H, ($C_{6''}$–C<u>H</u>)), 4.50 (s, 3H, ($C_{4''}$–C<u>H</u>$_3$)), 4.23 (dd, 1H, ($C_{3''}$–C<u>H</u>)), 3.68 (s, 5H, 5OH), 3.57 (d, 1H, J = 3.2, ($C_{5'}$–C<u>H</u>)), 3.51 (d, 2H, J = 3.2, (C_7-C<u>H</u>$_2$)), 3.29 (m, 1H, (C_{14}-C<u>H</u>)), 3.26 (m, 1H, (C_5-C<u>H</u>)), 2.46 (m, 1H, ($C_{4''}$–C<u>H</u>)), 2.41 (s, 3H, (N_6-C<u>H</u>$_3$), 2.22 (s, 6H, ($C_{4''}$-N(C<u>H</u>$_3$)$_2$), 2.04 (m, 1H, (C_{12}-C<u>H</u>)), 2.01 (d, 2H, J = 5.4, (C_9-C<u>H</u>$_2$)), 1.87 (dd, 2H, ($C_{5''}$–C<u>H</u>$_2$)), 1.79 (m, 1H, (C_8-C<u>H</u>)), 1.77 (d, 2H, ($C_{3'}$–C<u>H</u>$_2$)), 1.54 (m, 2H, (C_2-C<u>H</u>$_2$CH$_3$)), 1.40 (d, 3H, J = 3.2, ($C_{6'}$–C<u>H</u>$_3$)), 1.38 (s, 3H, (C_{10}-C<u>H</u>$_3$)), 1.22 (s, 3H, ($C_{4'}$–C<u>H</u>$_3$)), 1.11 (d, 3H, J = 4.8, ($C_{6''}$–C<u>H</u>$_3$)), 1.09 (d, 3H, (C_{14}-C<u>H</u>$_3$)), 1.08 (d, 3H, J = 5.3, (C_{12}-C<u>H</u>$_3$)), 1.00 (s, 3H, (C_3-C<u>H</u>$_3$)), 0.95 (d, 3H, (C_5-C<u>H</u>$_3$)), 0.88 (d, 3H, J = 3.4, (C_8-C<u>H</u>$_3$)), 0.83 (t, 3H, (C_2-CH$_2$C<u>H</u>$_3$)). ^{13}C NMR data (100 MHz, DMSO d_6) (ppm): δ = 176.9 (C_{15}-<u>C</u> = O), 169.9 (TCNQ 2 ring <u>C</u> = C-CN), 134.7 (TCNQ 4 ring <u>C</u>), 114.2 (4CN), 102.8 ($C_{2''}$–<u>C</u>H), 94.71 ($C_{2'}$–<u>C</u>H), 83.60 (C_{11}-<u>C</u>), 80.66 (TCNQ = <u>C</u>-CN), 77.36 (C_4-<u>C</u>H), 77.21 (C_{13}-<u>C</u>), 75.34 ($C_{5'}$–<u>C</u>H), 74.84 (C_2-<u>C</u>H), 74.50 (C_{10}-<u>C</u>), 74.26 ($C_{4'}$-<u>C</u>), 73.65 (C_3-<u>C</u>), 72.85 ($C_{3''}$–<u>C</u>H), 69.99 ($C_{6''}$–<u>C</u>H), 66.66 ($C_{4''}$–<u>C</u>H), 65.16 (C_6–<u>C</u>H), 62.61 (C_5-<u>C</u>H), 61.01 (C_7-<u>C</u>H$_2$), 49.90 ($C_{4'}$–O<u>C</u>H$_3$), 49.58 (C_{14}-<u>C</u>H), 49.13 (N_6-<u>C</u>H$_3$), 45.65 ($C_{3''}$-*N*(2<u>C</u>H$_3$)), 42.79 (C_{12}-<u>C</u>H), 36.50 (C_9-<u>C</u>H), 36.33 ($C_{3'}$–<u>C</u>H$_2$), 34.90 (C_8-<u>C</u>H), 31.38 ($C_{5''}$–<u>C</u>H$_2$), 25.91 (C_{10}-<u>C</u>H$_3$), 25.39 ($C_{4'}$–<u>C</u>H$_3$), 22.80 (C_2-<u>C</u>H$_2$CH$_3$), 21.45 ($C_{6''}$–<u>C</u>H$_3$), 21.18 (C_8-<u>C</u>H$_3$), 21.06 (C_3-<u>C</u>H$_3$), 18.81 (C_6–<u>C</u>H$_3$), 17.04 (C_{15}-<u>C</u>H$_3$), 11.50 (C_5-<u>C</u>H$_3$), 9.11 (C_2-CH$_2$<u>C</u>H$_3$), 8.33 (C_{12}-<u>C</u>H$_3$).

3.3.3. DDQ complex

Dark brown-colored powder; yield 92%; CHN elemental data: $C_{46}H_{72}Cl_2N_4O_{14}$ (975.98 g mol^{-1}); Observed (%): C 56.34; H 7.56;

N 5.95. Calculated (%): C 56.56; H 7.38; N 5.74. UV–visible data (nm): 293, 346, 460. FTIR data (cm^{-1}): 472, 570, 734, 803, 853, 901, 995, 1040, 1170, 1266, 1374, 1462, 1535, 1656, 1719, 2219, 2277, 2840, 2879, 2935, 2965, 3238, 3483. ^{1}H NMR data (400 MHz, DMSO d_6) (ppm): δ = 5.69 (t, 1H, (C_2-C<u>H</u>)), 5.64 (t, 1H, ($C_{2''}$–C<u>H</u>)), 5.38 (d, 1H, ($C_{2''}$–C<u>H</u>)), 5.14 (m, 1H, ($C_{6''}$–C<u>H</u>)), 5.01 (dd, 1H, (C_{13}-C<u>H</u>)), 4.71 (d, 1H, J = 4.8, (C_{11}-C<u>H</u>)), 4.60 (d, 1H, J = 5.2, (C_4-C<u>H</u>)), 4.56 (m, 1H, ($C_{6''}$–C<u>H</u>)), 4.30 (s, 3H, ($C_{4'}$–C<u>H</u>$_3$)), 4.27 (dd, 1H, ($C_{3''}$–C<u>H</u>)), 3.67 (s, 5H, 5OH), 3.45 (d, 1H, J = 3.6, ($C_{5'}$–C<u>H</u>)), 3.31 (d, 2H, J = 3.1, (C_7-C<u>H</u>$_2$)), 3.26 (m, 1H, (C_{14}-C<u>H</u>)), 3.01 (m, 1H, (C_5-C<u>H</u>)), 2.97 (m, 1H, ($C_{4''}$–C<u>H</u>)), 2.81 (s, 3H, (N_6-C<u>H</u>$_3$), 2.78 (s, 6H, ($C_{4''}$-N(C<u>H</u>$_3$)$_2$), 2.25 (m, 1H, (C_{12}-C<u>H</u>)), 2.22 (d, 2H, J = 4.4, (C_9-C<u>H</u>$_2$)), 2.20 (dd, 2H, ($C_{5''}$–C<u>H</u>$_2$)), 1.84 (m, 1H, (C_8-C<u>H</u>)), 1.70 (d, 2H, ($C_{3''}$–C<u>H</u>$_2$)), 1.55 (m, 2H, (C_2-C<u>H</u>$_2$CH$_3$)), 1.53 (d, 3H, J = 3.6, ($C_{6'}$–C<u>H</u>$_3$)), 1.22 (s, 3H, (C_{10}-C<u>H</u>$_3$)), 1.20 (s, 3H, ($C_{4'}$–C<u>H</u>$_3$)), 1.17 (d, 3H, J = 4.8, ($C_{6''}$–C<u>H</u>$_3$)), 1.10 (d, 3H, (C_{14}-C<u>H</u>$_3$)), 1.04 (d, 3H, J = 5.4, (C_{12}-C<u>H</u>$_3$)), 0.99 (s, 3H, (C_3-C<u>H</u>$_3$)), 0.95 (d, 3H, (C_5-C<u>H</u>$_3$)), 0.85 (d, 3H, J = 3.6, (C_8-C<u>H</u>$_3$)), 0.81 (t, 3H, (C_2-CH$_2$C<u>H</u>$_3$)). ^{13}C NMR data (100 MHz, DMSO d_6) (ppm): δ = 177.9 (C_{15}-<u>C</u> = O), 154.2 (DDQ 2C = O), 141.7 (DDQ 2*C*-Cl), 129.1 (DDQ 2*C*-CN), 116.6 (2CN), 101.7 ($C_{2''}$–<u>C</u>H), 94.71 ($C_{2''}$–<u>C</u>H), 83.60 (C_{11}-<u>C</u>), 77.81 (C_4-<u>C</u>H), 77.21 (C_{13}-<u>C</u>), 75.34 ($C_{5''}$–<u>C</u>H), 74.99 (C_2-<u>C</u>H), 74.76 (C_{10}-<u>C</u>), 74.66 ($C_{4''}$-<u>C</u>), 73.65 (C_3-<u>C</u>), 72.85 ($C_{3''}$–<u>C</u>H), 69.39 ($C_{6''}$–<u>C</u>H), 66.80 ($C_{4''}$–<u>C</u>H), 65.37 ($C_{6'}$–<u>C</u>H), 62.61 (C_5-<u>C</u>H), 61.01 (C_7-<u>C</u>H$_2$), 49.91 ($C_{4'}$–O<u>C</u>H$_3$), 49.58 (C_{14}-<u>C</u>H), 49.13 (N_6-<u>C</u>H$_3$), 45.65 ($C_{3''}$-*N*(2<u>C</u>H$_3$)), 42.79 (C_{12}-<u>C</u>H), 36.76 (C_9-<u>C</u>H), 36.33 ($C_{3'}$–<u>C</u>H$_2$), 34.90 (C_8-<u>C</u>H), 31.38 ($C_{5''}$–<u>C</u>H$_2$), 25.50 (C_{10}-<u>C</u>H$_3$), 25.26 ($C_{4'}$–<u>C</u>H$_3$), 22.84 (C_2-<u>C</u>H$_2$CH$_3$), 21.74 ($C_{6''}$–<u>C</u>H$_3$), 21.35 (C_8-<u>C</u>H$_3$), 21.32 (C_3-<u>C</u>H$_3$), 18.17 ($C_{6'}$–<u>C</u>H$_3$), 17.09 (C_{15}-<u>C</u>H$_3$), 11.71 (C_5-<u>C</u>H$_3$), 9.85 (C_2-CH$_2$<u>C</u>H$_3$), 9.01 (C_{12}-<u>C</u>H$_3$),

3.3.4. TFQ complex

Light violet-colored powder; yield 94%; CHN elemental data: $C_{44}H_{72}F_4N_2O_{14}$ (929.04 g mol^{-1}); Observed (%): C 57.03; H 7.55; N 3.28. Calculated (%): C 56.83; H 7.75; N 3.01. UV–visible data (nm): 296, 400. FTIR data (cm^{-1}): 467, 555, 633, 740, 907, 999, 1048, 1090, 1171, 1333, 1378, 1460, 1549, 1690, 2833, 2882, 2930, 2970, 3371, 3478. ^{1}H NMR data (400 MHz, DMSO d_6) (ppm): δ = 5.68 (t, 1H, (C_2-C<u>H</u>)), 5.60 (t, 1H, ($C_{2''}$–C<u>H</u>)), 5.43 (d, 1H, ($C_{2''}$–C<u>H</u>)), 5.12 (m, 1H, ($C_{6''}$–C<u>H</u>)), 4.91 (dd, 1H, (C_{13}-C<u>H</u>)), 4.86 (d, 1H, J = 5.4, (C_{11}-C<u>H</u>)), 4.83 (d, 1H, J = 5.6, (C_4-C<u>H</u>)), 4.69 (m, 1H, ($C_{6''}$–C<u>H</u>)), 4.58 (s, 3H, ($C_{4'}$–C<u>H</u>$_3$)), 4.47 (dd, 1H, ($C_{3''}$–C<u>H</u>)), 3.79 (s, 5H, 5OH), 3.58 (d, 1H, J = 3.2, ($C_{5'}$–C<u>H</u>)), 3.37 (d, 2H, J = 3.4, (C_7-C<u>H</u>$_2$)), 3.25 (m, 1H, (C_{14}-C<u>H</u>)), 3.14 (m, 1H, (C_5-C<u>H</u>)), 2.96 (m, 1H, ($C_{4''}$–C<u>H</u>)), 2.75 (s, 3H, (N_6-C<u>H</u>$_3$), 2.65 (s, 6H, ($C_{4''}$-N(C<u>H</u>$_3$)$_2$), 2.53 (m, 1H, (C_{12}-C<u>H</u>)), 2.22 (d, 2H, J = 5.4, (C_9-C<u>H</u>$_2$)), 1.99 (dd, 2H, ($C_{5''}$–C<u>H</u>$_2$)), 1.87 (m, 1H, (C_8-C<u>H</u>)), 1.73 (d, 2H, ($C_{3'}$–C<u>H</u>$_2$)), 1.51 (m, 2H, (C_2-C<u>H</u>$_2$CH$_3$)), 1.47 (d, 3H, J = 3.4, ($C_{6'}$–C<u>H</u>$_3$)), 1.33 (s, 3H, (C_{10}-C<u>H</u>$_3$)), 1.26 (s, 3H, ($C_{4'}$–C<u>H</u>$_3$)), 1.11 (d, 3H, J = 4.4, ($C_{6''}$–C<u>H</u>$_3$)), 1.09 (d, 3H, (C_{14}-C<u>H</u>$_3$)), 1.04 (d, 3H, J = 5.4, (C_{12}-C<u>H</u>$_3$)), 0.99 (s, 3H, (C_3-C<u>H</u>$_3$)), 0.96 (d, 3H, (C_5-C<u>H</u>$_3$)), 0.87 (d, 3H, J = 3.2, (C_8-C<u>H</u>$_3$)), 0.85 (t, 3H, (C_2-CH$_2$C<u>H</u>$_3$)). ^{13}C NMR data (100 MHz, DMSO d_6) (ppm): δ = 177.8 (Floranil C = O), 175.6 (C_{15}-<u>C</u> = O), 148.7 (Floranil 4*C*-F), 101.3 ($C_{2''}$–<u>C</u>H), 94.73 ($C_{2''}$–<u>C</u>H), 83.66 (C_{11}-<u>C</u>), 77.84 (C_4-<u>C</u>H), 77.53 (C_{13}-<u>C</u>), 75.33 ($C_{5''}$–<u>C</u>H), 74.99 (C_2-<u>C</u>H), 74.71 (C_{10}-<u>C</u>), 74.25 ($C_{4''}$-<u>C</u>), 73.61 (C_3-<u>C</u>), 72.13 ($C_{3''}$–<u>C</u>H), 69.09 ($C_{6''}$–<u>C</u>H), 66.39 ($C_{4''}$–<u>C</u>H), 65.38 ($C_{6'}$–<u>C</u>H), 62.13 (C_5-<u>C</u>H), 61.34 (C_7-<u>C</u>H$_2$), 49.61 ($C_{4'}$–O<u>C</u>H$_3$), 49.52 (C_{14}-<u>C</u>H), 45.39 (N_6-<u>C</u>H$_3$), 42.21 ($C_{3''}$-*N*(2<u>C</u>H$_3$)), 39.17 (C_{12}-<u>C</u>H), 36.06 (C_9-<u>C</u>H), 34.65 ($C_{3'}$–<u>C</u>H$_2$), 31.81 (C_8-<u>C</u>H), 25.95 ($C_{5''}$–<u>C</u>H$_2$), 25.47 (C_{10}-<u>C</u>H$_3$), 22.21 ($C_{4'}$–<u>C</u>H$_3$), 21.80 (C_2-<u>C</u>H$_2$CH$_3$), 21.37 ($C_{6''}$–<u>C</u>H$_3$), 21.16 (C_8-<u>C</u>H$_3$), 18.85 (C_3-<u>C</u>H$_3$), 18.39 ($C_{6'}$–<u>C</u>H$_3$), 15.71 (C_{15}-<u>C</u>H$_3$), 11.60 (C_5-<u>C</u>H$_3$), 9.41 (C_2-CH$_2$<u>C</u>H$_3$), 8.15 (C_{12}-<u>C</u>H$_3$),

3.4. Elemental and UV–visible spectral results

The elemental results for the synthesized CTCs indicated that the solid–solid interaction between azithromycin and the TCNQ, DDQ, and TFQ acceptors proceeded at a molar ratio of 1:1. This molar ratio agreed with that obtained in solution using both the spectrophotometric titration and Job's continuous variation methods. The UV–visible spectra of the CTCs dissolved in methanol solvent at a concentration of 5.0×10^{-4} in the 200 to 800 nm region are presented in Figs. 9a-c. The UV–visible absorption spectrum of azithromycin complexed with the TCNQ acceptor was characterized by a sole, very strong, broad band ranging from 286 to 380 nm with a λ_{max} of 336 nm. The UV–visible spectrum of the DDQ complex was characterized by three absorption bands: a very strong, sharp band at 293 nm, a small band detected at 346 nm, and a wide, medium-intensity band ranging from 370 to 600 nm with a λ_{max} of 460 nm. The spectrum of the complex with the TFQ acceptor contained a narrow, high-intensity band at 296 nm and a wide, low-intensity band centered at 400 nm. The shapes of the UV–visible absorption spectra of the synthesized CTCs were similar to those of the CTCs produced by mixing methanolic solutions of azithromycin and the acceptors at 1:1 (Fig. 5), with the same λ_{max} positions. The elemental and UV–visible spectral results confirmed that the solvent-free, solid–solid interactions between azithromycin and all of the acceptors produced the same CTCs generated by mixing methanolic solutions of azithromycin with each acceptor.

3.5. Infra-red spectral results

The free azithromycin molecule displayed the following characteristic IR bands: 570, 737, 797, 836, 895, 992, 1040, 1083, 1181, 1269, 1377, 1465, 1660, 1719, 2834, 2883, 2932, 2971, 3245, and 3490 cm^{-1}. The bands observed at 1181, 1083, 1040, and 992 cm^{-1} were caused by the ν_{as}(C – N), ν_s(C – N), ν(C – O), and ν(C – C) vibrational modes, respectively [69]. Among these modes, that resulting from the ν(C – O) appeared as a very strong band. The bands resonating at 1719 and 1660 cm^{-1} were caused by the ν_{as}(C = O) and ν_s(C = O) vibrations, respectively. The former appeared as a sharp, medium-strong band, while the latter appeared as a broad, weak band. The bands located at 570, 797, 1269, 1377, 2834, and 2932 cm^{-1} were assigned to the vibrational modes of the five methylene (CH_2) groups in the azithromycin molecule: δ_{twist}(CH_2), δ_{wag}(CH_2), δ_{rock}(CH_2), δ_{sciss}(CH_2), ν_s(CH_2), and ν_{as}(CH_2), respectively [67-73]. Those located at 2971, 2883, 1465, and 836 cm^{-1} resulted from the vibrational modes of the 14 methyl (CH_3) groups: ν_{as}(CH_3), ν_s(CH_3), δ_{rock}(CH_3), and δ_{wag}(-CH_3), respectively. The bands resonating at 737, 895, and 3245–3490 cm^{-1} were characteristic of the vibrational modes of the five O – H bonds in the molecule: out-of-plane bending, in-plane bending, and stretching vibrations, respectively [74]. The IR spectrum of the free TCNQ acceptor had absorption bands with wavenumbers (3050 and 2964), (2216 and 2964), 1533, 1350, (1118 and 1052), and 855 cm^{-1} attributed to the vibrational motions of ν_{as}(C – H) and ν_s(C – H), ν(C≡N), ν(C = C), δ(C – H) deformation, δ(C-C), and δ_{rock}(C – H), respectively. The IR spectrum of the free DDQ acceptor had absorption bands with wavenumbers 2238, 1675, 1557, (1263 and 1171), (798, 720, and 893) cm^{-1} attributed to the vibrational motions of ν(C≡N), ν(C = O), ν(C = C), δ(C-C), and ν(C-Cl), respectively. The free TFQ acceptor displayed three very

strong, intense bands located at 1680, 1320, and 988 cm^{-1} assigned to the vibrational motions of ν(C = O), ν(C = C), and ν (C-F), respectively.

The IR spectra of the synthesized CTCs contained all of the principal bands of azithromycin and the corresponding acceptor molecule. The ν(C = C) vibration resonated as a medium-strong band at 1533 cm^{-1} in free TCNQ, a strong band at 1557 cm^{-1} in free DDQ, and a very strong band at 1320 cm^{-1} in free TFQ. After complexation with azithromycin, the intensity of this band decreased and shifted to 1555 cm^{-1} in the TCNQ complex, 1535 cm^{-1} in the DDQ complex, and 1333 cm^{-1} in the TFQ complex. The TCNQ, DDQ, and TFQ acceptor molecules bear different types of electron-withdrawing groups. The TCNQ molecule has four cyano groups, the TFQ molecule has two carbonyl groups and four fluorine groups, while the DDQ molecule has two cyano groups, two carbonyl groups, and two chloro groups. These groups pull the electron density from the aromatic ring of the acceptor causing the molecule to be a strong, robust electron-accepting system. These electron-withdrawing groups were affected by the complexation with azithromycin. The ν(C≡N) vibration of free TCNQ appeared as a medium-strong band at 2216 cm^{-1} with a broad, weak shoulder band at 2964 cm^{-1}. In free DDQ, it appeared as a weak band at 2238 cm^{-1}. After TCNQ and DDQ interacted with azithromycin, this band shifted to 2224–2284 cm^{-1} in the TCNQ complex and 2277 cm^{-1} in the DDQ complex. In the free DDQ molecule, the ν(C = O) vibration was recorded at 1675 cm^{-1}, while in its complex with azithromycin, it registered at 1656 cm^{-1}. In the free TFQ molecule, the ν(C = O) vibration was recorded at 1680 cm^{-1}, while in the corresponding complex, this band overlapped. In the free DDQ molecule, the ν(C − Cl) vibrations were recorded at 893, 798, and 720 cm^{-1}, while in the corresponding complex, these were shifted to 901, 853, and 803 cm^{-1}. In the free TFQ molecule, the ν(C − F) vibration registered at 988 cm^{-1}, after complexation with azithromycin, it shifted to 999 cm^{-1} with decreased intensity. The shifting of the vibrations of withdrawing groups (−CN, −C = O, −Cl, or − F) induced by the increased electron density around the acceptor moiety (TCNQ, DDQ, or TFQ) resulted from the complexation between azithromycin and the acceptors. The asymmetric and symmetric vibrations of C − N registered at 1181 and 1083 cm^{-1} in the free azithromycin molecule; after complexation, these bands shifted to 1171 and 1090 cm^{-1} in the TFQ complex. The asymmetric mode of C − N was recorded at 1172 and 1170 cm^{-1} in the complexes with TCNQ and DDQ, respectively, while the symmetric mode of this band overlapped in both complexes. These observations suggested that the charge transferred from the N − atoms in the azithromycin molecule to the C = C moiety of the TCNQ, DDQ, and TFQ molecules, which represents a direct n → π* transition, as proposed in Fig. 12 [75-83].

3.6. NMR spectral results

The ^{1}H NMR spectrum of the free azithromycin molecule showed that it produced 33 protons. These protons were observed with the region of δ = 6.61–0.58 ppm. This region was crowded with triplets, doublets, and singlets from the − CH_3, −CH_2, and − CH protons. The ^{13}C NMR spectrum of the free azithromycin molecule showed that it produced 37 carbon resonances, which appeared in the δ = 177.66–9.36 ppm range. In the ^{1}H and ^{13}C NMR spectra of the synthesized CTCs, all of the carbon and proton resonances that characterized the free azithromycin molecule were detected. The complexation between azithromycin and all of the acceptors affected the protons of the tertiary amino group [−$N(CH_3)_2$] attached to carbon number $C_{4''}$, the tertiary amino group [>N − CH_3] and (OH) groups of the free azithromycin molecule. The protons of the [−$N(CH_3)_2$] group up-field shifted from 2.99 ppm in the free azithromycin molecule to 2.22, 2.78, and 2.65 ppm in its complexes with TCNQ, DDQ, and TFQ, respectively. The protons of the [>N − CH_3] group up-field shifted from 3.20 ppm in the free azithromycin molecule to 2.41, 2.81, and 2.75 ppm in its complexes with TCNQ, DDQ, and TFQ, respectively. The five protons from the (OH) groups exhibited a singlet at 4.33 ppm in free azithromycin; this signal shifted to 3.68, 3.67, and 3.79 ppm in its complexes with TCNQ, DDQ, and TFQ, respectively. The up-field chemical shifts of these protons were due to the presence of the n → π* transition between azithromycin and the acceptors. This transition affected the electronic environments of the azithromycin protons. The four protons of the TCNQ ring showed a singlet signal at 7.55 ppm in the TCNQ complex. The 37 carbon resonances of the free azithromycin molecule underwent several changes after its complexation with the acceptors. The TCNQ, DDQ, and TFQ complexes displayed 41, 41, and 39 resolved carbon signals in their ^{13}C NMR spectra, respectively, in agreement with the proposed structures illustrated in Fig. 12. The chemical shifts for the carbons in the withdrawing groups: −CN in the TCNQ complex was observed at δ 114.2 ppm. The chemical shift for carbons of withdrawing groups, C = O and − C − F, in the TFQ complex, were observed at δ 177.8 and 148.7 ppm, respectively. The carbons of the withdrawing groups − CN, C = O, and − C − Cl in the DDQ complex resonated at δ 116.6, 154.2, and 141.7 ppm, respectively. Carbon number $C_{4''}$ that carried the [−$N(CH_3)_2$] group resonated at δ 65.40 ppm in the free azithromycin molecule; after complexation, this signal shifted to δ 66.66, 66.80, and 66.39 ppm in the azithromycin-TCNQ, -DDQ, and -TFQ complexes, respectively.

4. Conclusions

Human coronavirus SARS-CoV-2, since December 2019, has led to a global pandemic with high morbidity and mortality. In response, numerous treatment options have been studied worldwide. One of these options is based on the broad-spectrum antibiotic azithromycin alone and in conjugation with other compounds. In this work, three CTCs of azithromycin with TCNQ, DDQ, and TFQ acceptors were produced by mortar-grinding at room temperature under solvent-free conditions. Color changes visible to the naked eye were seen when azithromycin formed soluble and solid CTCs with the investigated acceptors. Elemental and spectral analyses suggested that the interaction between azithromycin and all of the investigated acceptors involved a n → π* transition that proceeded at a 1:1 azithromycin to acceptor stoichiometry. The proposed protocol was rapid (5 min), effective, eco-friendly, reproducible, easily performed on a micro- or macroscale, required no specialized equipment, and generated the desired complexes with excellent yields (92–95%).

CRediT authorship contribution statement

Abdel Majid A. Adam: Data curation, Funding acquisition, Project administration, Writing - original draft, Writing - review & editing. **Hosam A. Saad:** Supervision, Conceptualization, Software, Validation, Visualization. **Amnah M. Alsuhaibani:** Investigation, Formal analysis, Methodology, Resources. **Moamen S. Refat:** Supervision, Conceptualization, Software, Validation, Visualization. **Mohamed S. Hegab:** Investigation, Formal analysis, Methodology, Resources.

Declaration of Competing Interest

The authors declare that they have no known competing financial interests or personal relationships that could have appeared to influence the work reported in this paper.

Acknowledgments

This work was supported by Taif University Researchers Supporting Project Number (TURSP-2020/02), Taif University, Taif, Saudi Arabia. The authors are very grateful to Dr. Leah Boyer (San Diego, CA, USA) for reviewing and editing the manuscript.

Appendix A. Supplementary data

Supplementary data to this article can be found online at https://doi.org/10.1016/j.molliq.2021.116250.

References

[1] M. Alkotaji, Azithromycin and ambroxol as potential pharmacotherapy for SARS-CoV-2, Int. J. Antimicrob. Agents 56 (6) (2020) 106192.
[2] Y. Zheng, J. Shang, Y. Yang, C. Liu, Y. Wan, Q. Geng, M. Wang, R. Baric, F. Li, Lysosomal proteases are a determinant of coronavirus tropism, J. Virol. 92 (2018) e01504–e1518.
[3] J. Andreani, M. Le Bideau, I. Duflot, P. Jardot, C. Rolland, M. Boxberger, N. Wurtz, J-. Rolain, P. Colson, B. La Scola, D. Raoult, *In vitro* testing of combined hydroxychloroquine and azithromycin on SARS-CoV-2 shows synergistic effect, Microb. Pathog. 145 (2020) 104228.
[4] N. Zhu, D. Zhang, W. Wang, X. Li, B. Yang, J. Song, X. Zhao, B. Huang, W. Shi, R. Lu, P. Niu, F. Zhan, X. Ma, D. Wang, W. Xu, G. Wu, G.F. Gao, D. Phil. W. Tan, A novel coronavirus from patients with pneumonia in China, 2019, N. Engl. J. Med. 382 (2020) 727-733.
[5] W.H. Organization, WHO director-General's opening remarks at the media briefing on COVID-19, 11 March 2020, Switzerland, Geneva, 2020.
[6] A. Firth, P. Prathapan, Azithromycin: The first broad-spectrum therapeutic, European J. Med. Chem. 207 (2020) 112739.
[7] P. Zarogoulidis, N. Papanas, I. Kioumis, E. Chatzaki, E. Maltezos, K. Zarogoulidis, Macrolides: from in vitro anti-inflammatory and immunomodulatory properties to clinical practice in respiratory diseases, Eur. J. Clin. Pharmacol. 68 (5) (2012) 479–503.
[8] J. Min, Y.J. Jang, Macrolide therapy in respiratory viral infections, Mediators Infamm. 2012 (2012) 649570.
[9] I. Grgičević, I. Mikulandra, M. Bukvić, M. Banjanac, V. Radovanović, I. Habinovec, B. Bertoša, P. Novak, Discovery of macrozones, new antimicrobial thiosemicarbazone-based azithromycin conjugates: design, synthesis and in vitro biological evaluation, Int. J. Antimicrob. Agents 56 (5) (2020) 106147.
[10] T. Fiolet, A. Guihur, M.E. Rebeaud, M. Mulot, N. Peiffer-Smadja, Y. Mahamat-Saleh, Effect of hydroxychloroquine with or without azithromycin on the mortality of coronavirus disease 2019 (COVID-19) patients: a systematic review and meta-analysis, Clin. Microbiol. Infect. 27 (1) (2021) 19–27.
[11] K. Maneikis, U. Ringeleviciute, J. Bacevicius, E. Dieninyte-Misiune, E. Burokaite, G. Kazbaraite, M.M. Janusaite, A. Dapkeviciute, A. Zucenka, V. Peceliunas, L. Kryzauskaite, V. Kasiulevicius, D. Ringaitiene, B. Zablockiene, T. Zvirblis, G. Marinskis, L. Jancoriene, L. Griskevicius, Mitigating arrhythmia risk in Hydroxychloroquine and Azithromycin treated COVID-19 patients using arrhythmia risk management plan, IJC Heart Vasc. 32 (2021) 100685.
[12] I. Ali, O.M.L. Alharbi, COVID-19: Disease, management, treatment, and social impact, Sci. Total Environ. 728 (2020) 138861.
[13] N. Bakhshaliyev, M. Uluganyan, A. Enhos, E. Karacop, R. Ozdemir, The effect of 5-day course of hydroxychloroquine and azithromycin combination on QT interval in non-ICU COVID19(+) patients, J. Electrocardiol. 62 (2020) 59–64.
[14] P. Gautret, J. Lagier, P. Parola, V.T. Hoang, L. Meddeb, M. Mailhe, B. Doudier, J. Courjon, V. Giordanengo, V.E. Vieira, H.T. Dupont, S. Honoré, P. Colson, E. Chabrière, B. La Scola, J. Rolain, P. Brouqui, D. Raoult, Hydroxychloroquine and azithromycin as a treatment of COVID-19: results of an open-label non-randomized clinical trial, Int. J. Antimicrob. Agents 56 (1) (2020) 105949.
[15] A. Pain, M. Lauriola, A. Romandini, F. Scaglione, Macrolides and viral infections: focus on azithromycin in COVID-19 pathology, Int. J. Antimicrob. Agents 56 (2) (2020) 106053.
[16] S.M. Vouri, T.N. Thai, A.G. Winterstein, An evaluation of co-use of chloroquine or hydroxychloroquine plus azithromycin on cardiac outcomes: A pharmacoepidemiological study to inform use during the COVID19 pandemic, Res. Social. Adm. Pharm. 17 (1) (2020) 2012–2017.
[17] R.L. Mitra, S.A. Greenstein, L.M. Epstein, An algorithm for managing QT prolongation in coronavirus disease 2019 (COVID-19) patients treated with either chloroquine or hydroxychloroquine in conjunction with azithromycin: Possible benefits of intravenous lidocaine, HeartRhythm Case Rep. 6 (5) (2020) 244–248.
[18] S. Arshad, P. Kilgore, Z.S. Chaudhry, G. Jacobsen, D.D. Wang, K. Huitsing, I. Brar, G.J. Alangaden, M.S. Ramesh, J.E. McKinnon, W. O'Neill, M. Zervos, Treatment with hydroxychloroquine, azithromycin, and combination in patients hospitalized with COVID-19, Int. J. Infect. Dis. 97 (2020) 396–403.
[19] Y. Liang, W. Xing, L. Liu, Y. Sun, W. Xu, D. Zhu, Charge transport behaviors of a novel 2:1 charge transfer complex based on coronene and $HAT(CN)_6$, Org. Electron. 78 (2020) 105608.
[20] G.G. Parra, A.L.S. Pavanelli, L.P. Franco, L.N.C. Máximo, R.S. da Silva, I. Borissevitch, Interaction of CdTe-MPA quantum dots with meso-tetra methyl pyridyl porphyrin. Charge transfer complex formation, J. Photochem. Photobiol., A 398 (2020) 112580.
[21] J. Li, X. Zhang, J. Nie, X. Zhu, Visible light and water-soluble photoinitiating system based on the charge transfer complex for free radical photopolymerization, J. Photochem. Photobiol., A 402 (2020) 112803.
[22] S. Lee, J. Hong, S. Jung, K. Ku, G. Kwon, W.M. Seong, H. Kim, G. Yoon, I. Kang, K. Hong, H.W. Jang, K. Kang, Charge-transfer complexes for high-power organic rechargeable batteries, Energy Storage Mater. 20 (2019) 462–469.
[23] T. Salzillo, N. Crivillers, M. Mas-Torrent, K. Wurst, J. Veciana, Synthesis of a vinylogue tetrathiafulvalene derivative and study of its charge transfer complex with $TCNQF_4$, Synth. Met. 247 (2019) 144–150.
[24] X. Chen, H. Wang, B. Wang, Y. Wang, X. Jin, F. Bai, Charge transport properties in organic D-A mixed-stack complexes based on corannulene and sumanene derivatives-a theoretical study, Org. Electron. 68 (2019) 35–44.
[25] G. Kang, S. He, H. Cheng, X. Ren, Enhanced intramolecular charge transfer of organic dyes containing hydantoin donor: A DFT study, J. Photochem. Photobiol., A 383 (2019) 111979.
[26] L. Man, T. Li, X. Wu, K. Lu, L. Yang, X. Liu, Z. Yang, J. Zhou, C. Ni, Synthesis, crystal structure, vibrational spectra, nonlinear optical property of an organic charge-transfer compound-4-nitrobenzyl isoquinolinium picrate based on DFT calculations, J. Mol. Struct. 1175 (2019) 971–978.
[27] M.V. Rusalov, V.V. Volchkov, V.L. Ivanov, M.Ya. Melnikov, F.E. Gostev, V.A. Nadtochenko, A.I. Vedernikov, S.P. Gromov, M.V. Alfimov, Ultrafast excited state dynamics of a stilbene–viologen charge transfer complex and its interaction with alkanediammonium salts, J. Photochem. Photobiol., A 372 (2019) 89–98.
[28] A.S.A. Almalki, A. Alhadhrami, A.M.A. Adam, I. Grabchev, M. Almeataq, J.Y. Al-Humaidi, T. Sharshar, M.S. Refat, Preparation of elastic polymer slices have the semiconductors properties for use in solar cells as a source of new and renewable energy, J. Photochem. Photobiol., A 361 (2018) 76–85.
[29] A.S.A. Almalki, A. Alhadhrami, R.J. Obaid, M.A. Alsharif, A.M.A. Adam, I. Grabchev, M.S. Refat, Preparation of some compounds and study their thermal stability for use in dye sensitized solar cells, J. Mol. Liq. 261 (2018) 565–582.
[30] I.M. Khan, M. Islam, S. Shakya, K. Alam, N. Alam, M. Shahid, Synthesis, characterization, antimicrobial and DNA binding properties of an organic charge transfer complex obtained from pyrazole and chloranilic acid, Bioorganic Chem. 99 (2020) 103779.
[31] I.M. Khan, S. Shakya, R. Akhtar, K. Alam, M. Islam, N. Alam, Exploring interaction dynamics of designed organic cocrystal charge transfer complex of 2-hydroxypyridine and oxalic acid with human serum albumin: Single crystal, spectrophotometric, theoretical and antimicrobial studies, Bioorganic Chem. 100 (2020) 103872.
[32] S. Niranjani, K. Venkatachalam, Synthesis, spectroscopic, thermal, structural investigations and biological activity studies of charge-transfer complexes of atorvastatin calcium with dihydroxy-*p*-benzoquinone, quinalizarin and picric acid, J. Mol. Struct. 1219 (2020) 128564.
[33] A. Karmakar, P. Bandyopadhyay, S. Banerjee, N.C. Mandal, B. Singh, Synthesis, spectroscopic, theoretical and antimicrobial studies on molecular charge-transfer complex of 4-(2-thiazolylazo)resorcinol (TAR) with 3, 5-dinitrosalicylic acid, picric acid, and chloranilic acid, J. Mol. Liq. 299 (2020) 112217.
[34] R. Kavitha, S. Nirmala, R. Nithyabalaji, R. Sribalan, Biological evaluation, molecular docking and DFT studies of charge transfer complexes of quinaldic acid with heterocyclic carboxylic acid, J. Mol. Struct. 1204 (2020) 127508.
[35] M.E. Mohamed, E.Y.Z. Frag, A.A. Hathoot, E.A. Shalaby, Spectrophotometric determination of fenoprofen calcium drug in pure and pharmaceutical preparations. Spectroscopic characterization of the charge transfer solid complexes, Spectrochim. Acta A 189 (2018) 357–365.
[36] O.R. Shehab, H. AlRabiah, H.A. Abdel-Aziz, G.A.E. Mostafa, Charge-transfer complexes of cefpodoxime proxetil with chloranilic acid and 2,3-dichloro-5,6-dicyano-1,4-benzoquinone: Experimental and theoretical studies, J. Mol. Liq. 257 (2018) 42–51.
[37] G.G. Mohamed, M.M. Hamed, N.G. Zaki, M.M. Abdou, M.E. Mohamed, A.M. Abdallah, Melatonin charge transfer complex with 2,3-dichloro-5,6-dicyano-1,4-benzoquinone: Molecular structure, DFT studies, thermal analyses, evaluation of biological activity and utility for determination of melatonin in pure and dosage forms, Spectrochim. Acta A 182 (2017) 143–159.
[38] N. Rahman, S. Sameen, M. Kashif, Spectroscopic study of charge transfer complexation between doxepin and π–acceptors and its application in quantitative analysis, J. Mol. Liq. 222 (2016) 944–952.
[39] A.M.A. Adam, M.S. Refat, H.A. Saad, Quick and simple formation of different nanosized charge-transfer complexes of the antibiotic drug moxifloxacin: An efficient way to remove and utilize discarded antibiotics, C.R, Chimie 18 (2015) 914–928.
[40] I.M. Khan, A. Ahmad, S. Kumar, Synthesis, spectroscopic characterization and structural investigations of a new charge transfer complex of 2,6-diaminopyridine with 3,5-dinitrobenzoic acid: DNA binding and antimicrobial studies, J. Mol. Struct. 1035 (2013) 38–45.
[41] A.M.A. Adam, M.S. Refat, A comparison of charge-transfer complexes of iodine with some antibiotics formed through two different approaches (liquid-liquid vs solid-solid), J. Mol. Liq. 329 (2021) 115560.
[42] A.M.A. Adam, M.S. Hegab, M.S. Refat, H. H.Eldaroti, Proton-transfer and charge-transfer interactions between the antibiotic trimethoprim and several σ- and

π- acceptors: A spectroscopic study, J. Mol. Struct. (2020) 129687, in press, https://doi.org/10.1016/j.molstruc.2020.129687
[43] C. Balraj, S. Balaji, M. Karthikeyan, Systematic measurements of charge transfer complexes caused from 1-phenyl-1,2,3,4-tetrahydroisoquinoline and 4-aminoacetanilide with series of π-acceptors (BQ, DDQ, TCNQ), Spectrochim. Acta A 245 (2021) 118931.
[44] A.A. El-Bindary, Z. Anwar, T. El-Shafaie, Effect of silicon dioxide nanoparticles on the assessment of quercetin flavonoid using Rhodamine B Isothiocyanate dye, J. Mol. Liq. 323 (2021) 114607.
[45] I.M. Khan, K. Alam, M.J. Alam, Exploring charge transfer dynamics and photocatalytic behavior of designed donor-acceptor complex: Characterization, spectrophotometric and theoretical studies (DFT/TD-DFT), J. Mol. Liq. 310 (2020) 113213.
[46] T.A. Altalhi, Utilization of tannic acid into spherical structured carbons based on charge-transfer complexation with tetracyanoethylene acceptor: Liquid-liquid and solid-solid interactions, J. Mol. Liq. 300 (2020) 112325.
[47] M.T. Basha, R.M. Alghanmi, S.M. Soliman, W.J. Alharby, Synthesis, spectroscopic, thermal, structural characterization and DFT/TD-DFT computational studies for charge transfer complexes of 2,4-diamino pyrimidine with some benzoquinone acceptors, J. Mol. Liq. 309 (2020) 113210.
[48] P.S. Koroteev, A.B. Ilyukhin, K.A. Babeshkin, N.N. Efimov, Charge transfer complexes of lanthanide 3,5-dinitrobenzoates and 1,2-phenylenediamine, J. Mol. Struct. 1207 (2020) 127800.
[49] A. El-Dissouky, T.E. Khalil, H.A. Elbadawy, D.S. El-Sayed, A.A. Attia, S. Foro, X-ray crystal structure, spectroscopic and DFT computational studies of H-bonded charge transfer complexes of tris (hydroxymethyl)aminomethane (THAM) with chloranilic acid (CLA), J. Mol. Struct. 1200 (2020) 127066.
[50] A.A. El-Bindary, E.A. Toson, K.R. Shoueir, H.A. Aljohani, M.M. Abo-Ser, Metal–organic frameworks as efficient materials for drug delivery: Synthesis, characterization, antioxidant, anticancer, antibacterial and molecular docking investigation, Appl. Organomet. Chem. 34 (2020) e5905.
[51] F.A. Al-Saif, A.A. El-Habeeb, M.S. Refat, H.H. Eldaroti, Majid A. Abdel, H. Adam, H.A.Sa.ad. Fetooh, Chemical and physical properties of the charge transfer complexes of domperidone antiemetic agent with π-acceptors, J. Mol. Liq. 293 (2019) 111517.
[52] F.A. Al-Saif, A.A. El-Habeeb, M.S. Refat, Majid A. Abdel, H.A. Adam, A.I. Saad, H. Fetooh El-Shenawy, Characterization of charge transfer products obtained from the reaction of the sedative-hypnotic drug barbital with chloranilic acid, chloranil, TCNQ and DBQ organic acceptors, J. Mol. Liq. 287 (2019) 110981.
[53] N. Venkatesh, B. Naveen, A. Venugopal, G. Suresh, V. Mahipal, P. Manojkumar, T. Parthasarathy, Donor-acceptor complex of 1-benzoylpiperazine with *p*-chloranil: Synthesis, spectroscopic, thermodynamic and computational DFT gas phase/PCM analysis, J. Mol. Struct. 1196 (2019) 462–477.
[54] U. Neupane, M. Singh, P. Pandey, R.N. Rai, Synthesis, spectroscopic, crystal structure, thermal and optical studies of a novel proton transfer complex: 2-Methyl-8-hydroxyquinoliniumpicrate, J. Mol. Struct. 1195 (2019) 131–139.
[55] W. Falek, R. Benali-Cherif, L. Golea, S. Samai, N. Benali-Cherif, E. Bendeif, I. Daoud, A structural comparative study of charge transfer compounds: Synthesis, crystal structure, IR, Raman-spectroscopy, DFT computation and hirshfeld surface analysis, J. Mol. Struct. 1192 (2019) 132–144.
[56] M. Faizan, Z. Afroz, M.J. Alam, V.H. Rodrigues, S. Ahmed, A. Ahmad, Structural, vibrational and electronic absorption characteristics of the monohydrate organic salt of 2-amino-5-bromo-6-methyl-4-pyrimidinol and 2,3-pyrazinedicarboxylic acid: A combined experimental and computational study, J. Mol. Struct. 1177 (2019) 229–241.
[57] K.S. Fathima, M. Sathiyendran, K. Anitha, Structure elucidation, biological evaluation and molecular docking studies of 3-aminoquinolinium 2-carboxy benzoate- A proton transferred molecular complex, J. Mol. Struct. 1176 (2019) 238–248.
[58] S. Soltani, P. Magri, M. Rogalski, M. Kadri, Charge-transfer complexes of hypoglycemic sulfonamide with π-acceptors: Experimental and DFT-TDDFT studies, J. Mol. Struct. 1175 (2019) 105–116.
[59] I.M. Khan, S. Shakya, N. Singh, Preparation, single-crystal investigation and spectrophotometric studies of proton transfer complex of 2,6-diaminopyridine with oxalic acid in various polar solvents, J. Mol. Liq. 250 (2018) 150–161.
[60] A.F. Shoair, A.A. El-Bindary, N.A. El-Ghamaz, G.N. Rezk, Synthesis, characterization, DNA binding and antitumor activities of Cu(II) complexes, J. Mol. Liq. 269 (2018) 619–638.
[61] A.S.A. Almalki, A.M. Naglah, M.S. Refat, M.S. Hegab, A.M.A. Adam, M.A. Al-Omar, Liquid and solid-state study of antioxidant quercetin donor and TCNE acceptor interaction: Focusing on solvent affect on the morphological properties, J. Mol. Liq. 233 (2017) 292–302.
[62] A.M.A. Adam, M.S. Refat, M.S. Hegab, H.A. Saad, Spectrophotometric and thermodynamic studies on the 1:1 charge transfer interaction of several clinically important drugs with tetracyanoethylene in solution-state: Part one, J. Mol. Liq. 224 (2016) 311–321.
[63] A.M.A. Adam, M.S. Refat, Solution and solid-state investigations of charge transfer complexes caused by the interaction of bathophenanthroline with different organic acceptors in a (methanol + dichloromethane) binary solvent system, J. Mol. Liq. 219 (2016) 377–389.
[64] A.M.A. Adam, M.S. Refat, H.A. Saad, M.S. Hegab, Charge transfer complexation of the anticholinergic drug clidinium bromide and picric acid in different polar solvents: Solvent effect on the spectroscopic and structural morphology properties of the product, J. Mol. Liq. 216 (2016) 192–208.
[65] A.M.A. Adam, H.A. Saad, A.M. Alsuhaibani, M.S. Refat, M.S. Hegab, Charge-transfer chemistry of azithromycin, the antibiotic used worldwide to treat the coronavirus disease (COVID-19). Part II: Complexation with several π-acceptors (PA, CLA, CHL), J. Mol. Liq. 325 (2021) 115121.
[66] A.M.A. Adam, H.A. Saad, A.M. Alsuhaibani, M.S. Refat, M.S. Hegab, Charge-transfer chemistry of azithromycin, the antibiotic used worldwide to treat the coronavirus disease (COVID-19). Part I: Complexation with iodine in different solvents, J. Mol. Liq. 325 (2021) 115187.
[67] D.A. Skoog, Principle of Instrumental Analysis, third ed., Saunders, New York, USA, 1985 (Chapter 7).
[68] K.S. Kumar, T. Parthasarathy, Synthesis, spectroscopic and computational studies of CT complexes of amino acids with iodine as σ Acceptor, J. Solut. Chem. 46 (2017) 1364–1403.
[69] D. Sajan, J. Binoy, B. Pradeep, K.V. Krishnan, V.B. Kartha, I.H. Joe, V.S. Jayakumar, NIR-FT Raman and infrared spectra and ab initio computations of glycinium oxalate, Spectrochim. Acta A 60 (2004) 173–180.
[70] D.N. Sathyanarayana, Vibrational Spectroscopy- Theory and Applications, second ed., New Age International (P) Limited Publishers, New Delhi, 2004.
[71] C. Sridevi, G. Velraj, Investigation of molecular structure, vibrational, electronic, NMR and NBO analysis of 5-chloro-1-methyl-4-nitro-1*H*-imidazole (CMNI) using ab initio HF and DFT calculations, J. Mol. Struct. 1019 (2012) 50–60.
[72] G. Socrates, Infrared and Raman Characteristic Group Frequencies-Tables and Charts, Third ed., Wiley, New York, 2001.
[73] G. Varsanyi, Assignments for Vibrational Spectra of Seven Hundred Benzene Derivatives, Vol. 1 and 2, Academic Kiado: Budapest, 1973.
[74] R.M. Silverstein, F.X. Webster, Spectrometric Identification of Organic Compounds, sixth ed., Jon Wiley Sons Inc., New York, 1963.
[75] A.M.A. Adam, H.H. Eldaroti, M.S. Hegab, M.S. Refat, J.Y. Al-Humaidi, H.A. Saad, Measurements and correlations in solution-state for charge transfer products caused from the 1:2 complexation of TCNE acceptor with several important drugs, Spectrochim. Acta A 211 (2019) 166–177.
[76] A.M.A. Adam, M.S. Refat, Chemistry of drug interactions: Characterization of charge-transfer complexes of Guaifenesin with various acceptors using spectroscopic and thermal methods, J. Gen. Chem. 84 (9) (2014) 1847–1856.
[77] A.M.A. Adam, Synthesis, spectroscopic, thermal and antimicrobial investigations of charge-transfer complexes formed from the drug procaine hydrochloride with quinol, picric acid and TCNQ, J. Mol. Struct. 1030 (2012) 26–39.
[78] H.H. Eldaroti, S.A. Gadir, M.S. Refat, A.M.A. Adam, Preparation, spectroscopic and thermal characterization of new charge-transfer complexes of ethidium bromide with π-acceptors. In vitro biological activity studies, Spectrochim. Acta A 109 (2013) 259–271.
[79] H.H. Eldaroti, S.A. Gadir, M.S. Refat, A.M.A. Adam, Spectroscopic investigations of the charge-transfer interaction between the drug reserpine and different acceptors: Towards understanding of drug–receptor mechanism, Spectrochim. Acta A 115 (2013) 309–323.
[80] H.H. Eldaroti, S.A. Gadir, M.S. Refat, A.M.A. Adam, Charge transfer complexes of the donor acriflavine and the acceptors quinol, picric acid, TCNQ and DDQ: Synthesis, spectroscopic characterizations and antimicrobial studies, Int. J. Electrochem. Sci. 8 (2013) 5774–5800.
[81] H.H. Eldaroti, S.A. Gadir, M.S. Refat, A.M.A. Adam, Charge-transfer interaction of drug quinidine with quinol, picric acid and DDQ: Spectroscopic characterization and biological activity studies towards understanding the drug–receptor mechanism, J. Pharm. Anal. 4 (2) (2014) 81–95.
[82] O.B. Ibrahim, E.A. Manaaa, M.M. AL-Majthoub, A.M. Fallatah, A.M.A. Adam, M. M. Alatibi, J.Y. Al-Humaidi, M.S. Refat, Estimation of metformin drug for the diabetes patients by simple, quick and cheap techniques within the formation of colored charge transfer complexes, Spectrosc. Spect. Anal. 38 (11) (2018) 3622-3630.
[83] M.S. Refat, O.B. Ibrahim, H.A. Saad, A.M.A. Adam, Usefulness of charge–transfer complexation for the assessment of sympathomimetic drugs: Spectroscopic properties of drug ephedrine hydrochloride complexed with some p-acceptors, J. Mol. Struct. 1064 (2014) 58–69.